JJEE

Volume 12 | Number 3 | September 2026 | Pages 505-522

Jordan Journal of Electrical Engineering

ISSN (print): 2409-9600, ISSN (online): 2409-9619

Homepage: jjee.ttu.edu.jo

Control of Antenna Tracker and Telemetry System for Unmanned Aerial Vehicle

Wahyudi[1*], Riezky Ramadhan[2], Yosua Alvin Adi Soetrisno[3]

[1, 2, 3] Electrical Engineering Department, Faculty of Engineering, Universitas Diponegoro, Semarang, Indonesia
E-mail: wahyuditinom@elektro.undip.ac.id

Received: Oct 04, 2025 Revised: Mar 25, 2026 Accepted: May 16, 2026 Available online: Aug 15, 2026

Abstract— For a mission to be successful, a long-range communication Unmanned Aerial Vehicles (UAVs) and Ground Control Stations (GCS) should be reliable. It is essential to ensure the success since it is necessary to obtain HD videos, high-bandwidth data. Therefore, developing an automated antenna tracking system is the aim of this study. The system utilizes a 5.8 GHz directional antenna, aiming to prevent the significant path loss associated with high-frequency bands. Proportional–Integral–Derivative (PID) controller becomes the basis of the system, generally optimized using Particle Swarm Optimization (PSO) with the Integral of Time weighted Squared Error (ITSE) as the objective function. Stationary step-response tests and autonomous flight missions were employed as experimental testing methods. The findings show that PSO optimized controller achieves superior stability with near-negligible overshoot and high pointing accuracy. Moreover, a tracking error below 0.5° across various UAV speeds is well maintained. Dealing with comparative field tests, the data suggest that the 5.8 GHz directional system keeps a robust data link up to 1 km. Thus, its performance is remarkably better than conventional 433 MHz omnidirectional setups which failed beyond 200 meters. Not only a practical, but also a feasible solution beneficial to boost telemetry range and stability in high-definition UAV monitoring applications.

Keywords— Antenna tracker; UAV; GCS; PSO; Telemetry system.

1. INTRODUCTION

UAVs have been excessively utilized across various critical missions. These missions, requiring real-time data acquisition and dependable communication links, deal with large-scale surveillance, disaster response, and even forest fire monitoring [1-6]. Thus, in order for these missions to be well-executed, the stability between the UAV and the GCS is highly required [7-9]. This type of communication architecture usually makes use of omnidirectional antennas on the UAV and high-gain directional antennas at the GCS, demanding an automated tracking system in order to maintain continuous alignment with the UAV's trajectory [10-12]. In its current modern UAV applications, high-definition (HD) video transmission with low latency is mandatory. The use of 433 MHz band, a conventional low frequency band, has limited bandwidth that HD streaming is not supported [13-15]. On the other hand, the 5.8 GHz frequency band shows greater throughput. However, path loss and limited coverage areas are likely to happen [16-19]. To address these limitations, there should be highly precise tracking accuracy to ensure that high gain antennas can maintain video link stability.

Earlier studies have been analyzed numerous control strategies for UAV antenna tracking such as Proportional-Integral (PI), Neuro Fuzzy System Controller (NFSC), PID, and Fuzzy PD-I [20-22]. The findings show that, under particular conditions, these methods are effective.

However, they depend on manual or heuristic tuning. Manual or heuristic tuning leads to suboptimal performance as it lacks systematic global optimization. Compared to conventional tuning, PSO, as one of promising optimization-based approaches, shows its superiority in reducing overshoot while enhancing transient response [24-25].

Most studies on antenna tracking constantly focused on low-frequency bands regardless advancements in control algorithms. Whereas, low-frequency bands do not support HD transmission [16,21,26]. Although propagation challenges are significantly more severe, studies on 5.8 GHz systems are still limited [27-28]. Thus, the main focus of this study is addressing the challenge in maintaining 5.8 GHz signal stability during dynamic UAV maneuvers, which often results in data loss due to tracking errors.

This study offers a novel integration an antenna tracking system for UAV–GCS communication at 5.8 GHz, with PID parameter optimization using the PSO method based on the ITSE criterion. The ITSE imposes a heavier penalty on errors occurring late in the response, maintaining the pointing accuracy. This study contributes to 1) the implementation of a stable 5.8 GHz system for HD video, 2) the comparative analysis between conventional and PSO-based PID tuning, and 3) the experimental validation demonstrating enhanced UAV–GCS alignment stability compared to standard omnidirectional systems.

2. METHODS

2.1. Antenna Tracker

The development of antenna tracker involved the use of a mechanical framework with two Degrees of Freedom (2-DoF). This mechanical framework can do a full 360° horizontal rotation on the azimuth (yaw) axis. It also facilitates a vertical range of 0° to 90° for the elevation (pitch) axis [29]. NEMA 23 stepper motors drive this dual-axis movement. 2:1 for the azimuth axis and 3:1 for the elevation axis are the specific gear ratios implemented. This enhances torque delivery and optimizes high resolution angular positioning. Fig. 1 shows the 3D model of the proposed tracker.

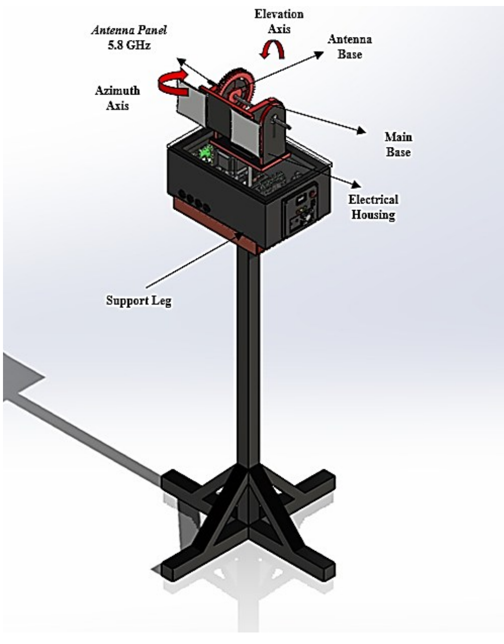

Fig. 1. Design of the proposed antenna tracker.

A main frame maintains the structural integrity of the system. The frame is supported by aluminum legs. Its main components are the antenna mount and holder fabricated from high-strength PLA+. A steel plate housing shields the electronic circuitry. Moreover, its configuration is designed to balance durability with operational portability.

Fig. 2 illustrates the hardware topology block diagram of the antenna tracker system. The main components of the angle control system include two XL4005 buck converters for stepping down the 12 V power supply, two AS5600 magnetic encoder sensors, a Teensy 4.1 microcontroller as the central controller, two TB6600 motor drivers, two NEMA 23 stepper motors as actuators for the azimuth and elevation axes, and two FY-05A high gain directional antennas operating at a frequency of 5.8 GHz.

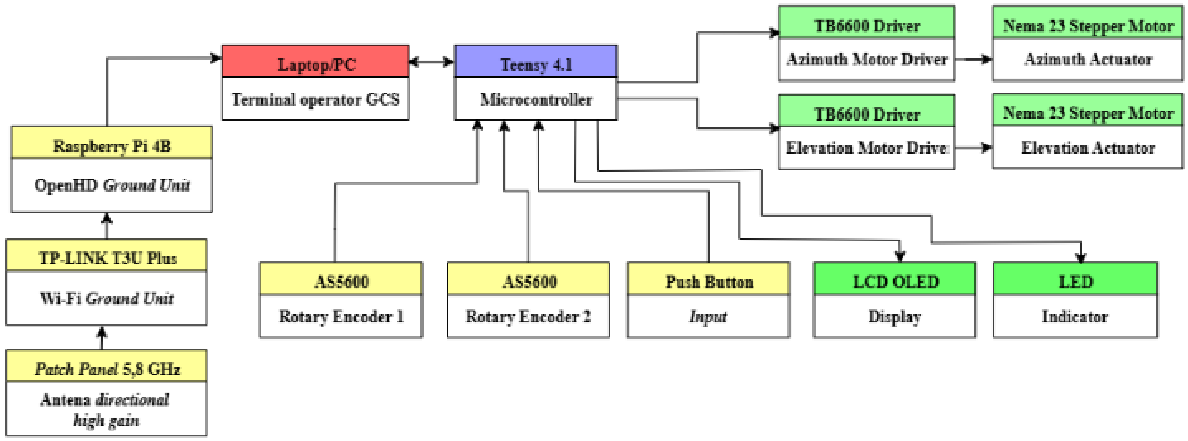

Fig. 2. Hardware topology block diagram of the antenna tracker system.

2.2. Unmanned Aerial Vehicle

The Pixhawk 5X is a flight controller in the UAV system. The controller maintains stability and controls UAV movement. The stability is maintained and the movement is controlled based on data from various sensors [30]. The Pixhawk 5X is connected to four Hobbywing 30A Electronic Speed Controllers (ESCs), each regulating the speed of a Tarot 5008 KV brushless motor. An M8N GPS equipped with a compass module is employed as the position sensor for navigation. Fig. 3 illustrates the physical implementation of the UAV platform and Fig. 4. shows the block diagram of the UAV system.

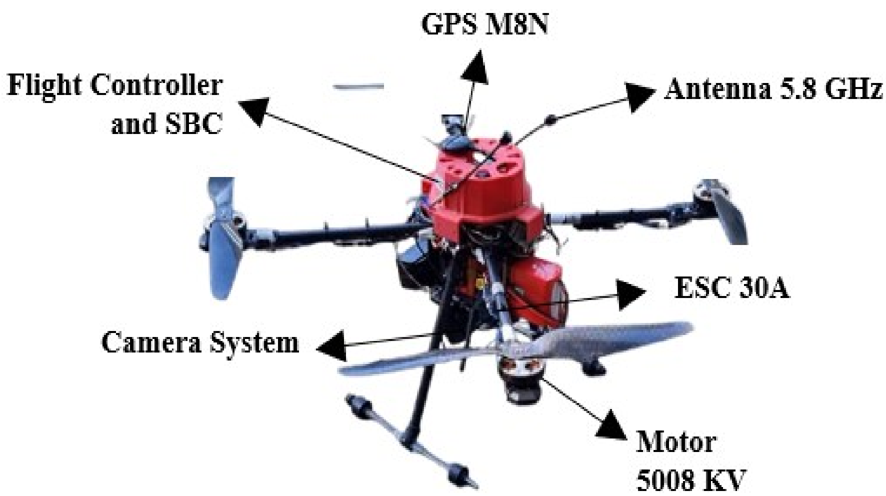

Fig. 3. Physical implementation of the UAV.

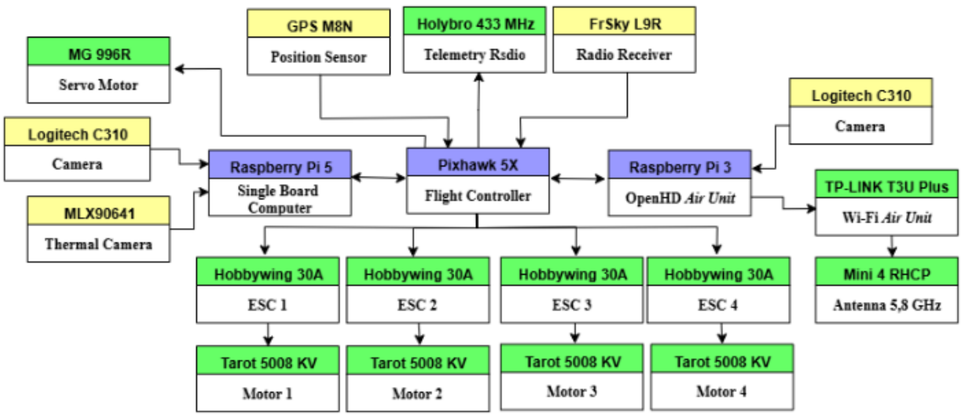

Fig. 4. Hardware topology block diagram of the UAV system.

2.3. Tracking System

In order to determine the antenna's orientation dynamically, the software architecture is developed through the processing of the UAV's real time spatial data, specifically its GPS coordinates and barometric altitude. The azimuth setpoint and the elevation setpoint are the two basis reference inputs for the control system. The computational workflow to get these setpoints is as follows:

A. Azimuth Setpoint Calculation

The target azimuth angle (z) is used to align the antenna with the UAV’s horizontal position relative to true north. It is calculated using bearing equations. First of all, the process determines the directional components X and Y in a two-dimensional horizontal plane using Eqs. (1) and (2):

$$X = cos\ \varphi_a . \sin(\lambda_a - \lambda_0) \quad (1)$$

$$Y = cos\ \varphi_0 . \sin\ \varphi_a - \sin\ \varphi_0 . \cos\ \varphi_a . \cos(\lambda_a - \lambda_0) \quad (2)$$

where φ_0, λ_0 represent the latitude and longitude of the GCS, and φ_a, λ_a represent the coordinates of the UAV. These components, representing the relative direction in a 2D plane, are then integrated using the two-argument inverse tangent function to provide a stable 360° heading as expressed in Eq. (3):

$$z = atan\,2(X, Y) \quad (3)$$

B. Elevation Setpoint Calculation

By utilizing the horizontal distance and altitude difference, trigonometric approach is used to determine the vertical orientation. Due to the potential for long distance operation, the horizontal distance (*d*) is calculated using the haversine formula. This formula considers the Earth a sphere with a radius of R = 6371km. This distance is based on the coordinate differences calculated in Eqs. (4) and (5):

$$\Delta\varphi = \varphi_a - \varphi_0 \quad (4)$$

$$\Delta\lambda = \lambda_a - \lambda_0 \quad (5)$$

The horizontal distance (*d*) is then obtained via the haversine equation in Eq. (6). The geometric relationship for this calculation, involving the altitude difference (*f*), is illustrated in Fig. 5.

$$d = 2.R.\arcsin(\sqrt{sin^2\left(\frac{\Delta\varphi}{2}\right) + cos\ (\varphi_0).\, cos\ (\varphi_1).\, sin^2\left(\frac{\Delta\lambda}{2}\right)} \quad (6)$$

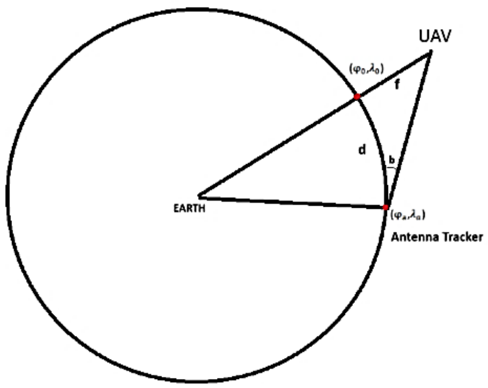

Fig. 5. Illustration of elevation angle calculation.

Finally, the elevation angle (*b*) is derived by incorporating the UAV altitude relative to the antenna tracker (*f*) as shown in Eq. (7):

$$b = tan^{-1}\left(\frac{f}{d}\right) \tag{7}$$

C. Position Control Logic

Reference angles for the PID-based position control system, ranging from 0° to 360° for the azimuth axis and 0° to 90° for the elevation axis are derived from the calculated setpoints. The system continuously computes errors by comparing these target angles against the actual positions reported by the AS5600 magnetic encoders. In order to obtain precise actuation commands for the stepper motors, the error signal is processed. Fig. 6 shows block diagram of azimuth axis controller.

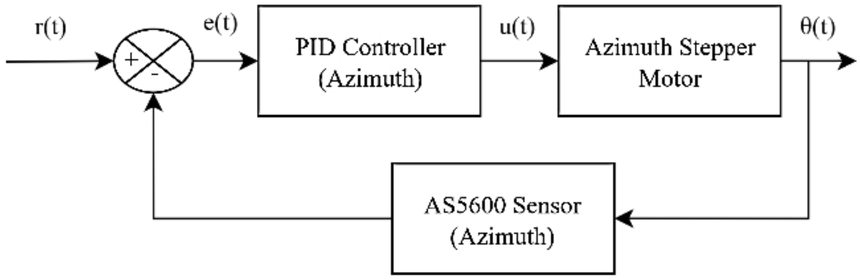

Fig. 6. Block diagram of azimuth axis controller.

2.4. Motor Control and Optimization Methodology

The control architecture for the antenna tracker's movement is developed using a stepper motor speed model from the MathWorks library as the simulation baseline. PID controller, implemented in a closed-loop configuration, helps achieve high-precision tracking. The parameters K_p, K_i, and K_d are optimized through the PSO algorithm [31, 32]. The tuning process is separately conducted since the azimuth and elevation axes operate under different mechanical conditions. Their payload mass and gear ratios are different. To ensure the results are applicable for real-world applications, the specific mass inertia for each axis was incorporated in the simulation environment. While the azimuth axis employs a 2:1 gear ratio, the elevation axis utilizes a 3:1 ratio. Fig. 7 displays Fig. 7. the simulink block diagram of PID tuning using the PSO method.

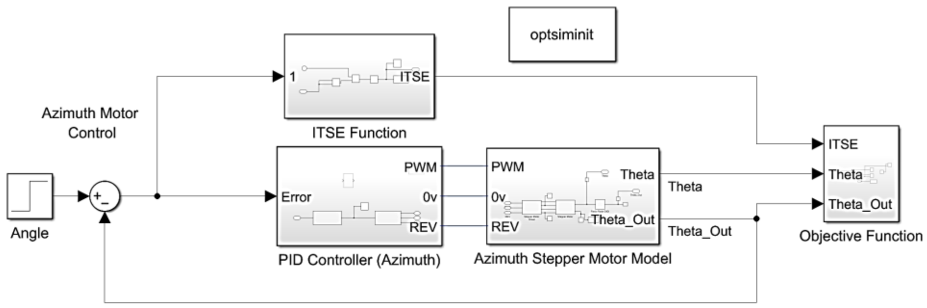

Fig. 7. Simulink block diagram of PID tuning using the PSO method.

A. PSO Tuning Procedure and Constriction Factor

The Constriction Factor Particle Swarm Optimization (CPSO) is employed in the tuning process. By doing so, algorithmic stability and convergence are ensured. Three decision variables ($nVar = 3$) that represent the PID gains become the focus of the optimization. To identify the most efficient swarm configuration, the number of particles varied between 2, 4, 6, and 8 across 30 iterations. Acceleration coefficients were maintained at $c_1 = 2$ and $c_2 = 2.05$.

A critical element in this methodology is the calculation of the constriction factor (χ), derived as follows:

$$\chi = \frac{2}{\left|2-\varphi-\sqrt{\varphi^2-4\varphi}\right|} \tag{8}$$

where $\varphi = C_1 + C_2$. This factor replaces the traditional inertia weight, providing superior control over the swarm's velocity and preventing numerical instability during the search process [33]. The operational flow of the PID optimization is detailed in the flowchart in Fig. 8

B. Objective Function and ITSE Justification.

A multi-criteria objective function (O) designed to minimize error and system instability evaluates the performance of each particle:

$$O = ITSE + 1.5\, overshoot + 10\, SSE \tag{9}$$

It is strategic to select of the ITSE for UAV antenna tracking over criteria such as IAE or ISE. While ISE equally penalizes all errors, ITSE considers a time-weighting factor (t). A time-weighting factor imposes a heavier penalty on errors occurring later in the response. For antenna tracker, achieving rapid initial movement is considered less essential compared to "pointing accuracy" once the UAV is in a steady state position. In order to maintain the narrow beamwidth alignment required by 5.8 GHz directional antennas, ITSE is required as it facilitates the PSO algorithm to prioritize solutions that eliminate residual errors and prevent long-term drifting.

C. Swarm Dynamics and Parameter Selection

Once all particles in an iteration are evaluated, both the velocity and position of each to explore the search space for the optimal gains are updated by the algorithm. Eqs. (10) and (11) govern the mechanism of the update:

$$v_{i,m}(t+1) = \chi\,[v_i(t) + c_1\, r_1\big(pBest_i - x_i(t)\big) + c_2\, r_2\,\Big(gBest - x_{i,}(t)\Big)] \tag{10}$$

$$x_{i,m}(t+1) = x_{i,m}(t) + v_{i,m}(t+1) \tag{11}$$

Precisely, article positions are constrained within predefined search boundaries based on the motor's dynamic properties to confirm the physical feasibility. For the azimuth axis, upper bounds were established at [30, 0.1, 0.1], while the elevation axis was restricted to [15, 0.1, 0.1].

The final optimal configuration is determined by the Global Best ($gBest$) particle that achieves the minimum ITSE value, as detailed in Table 1 and Table 2.

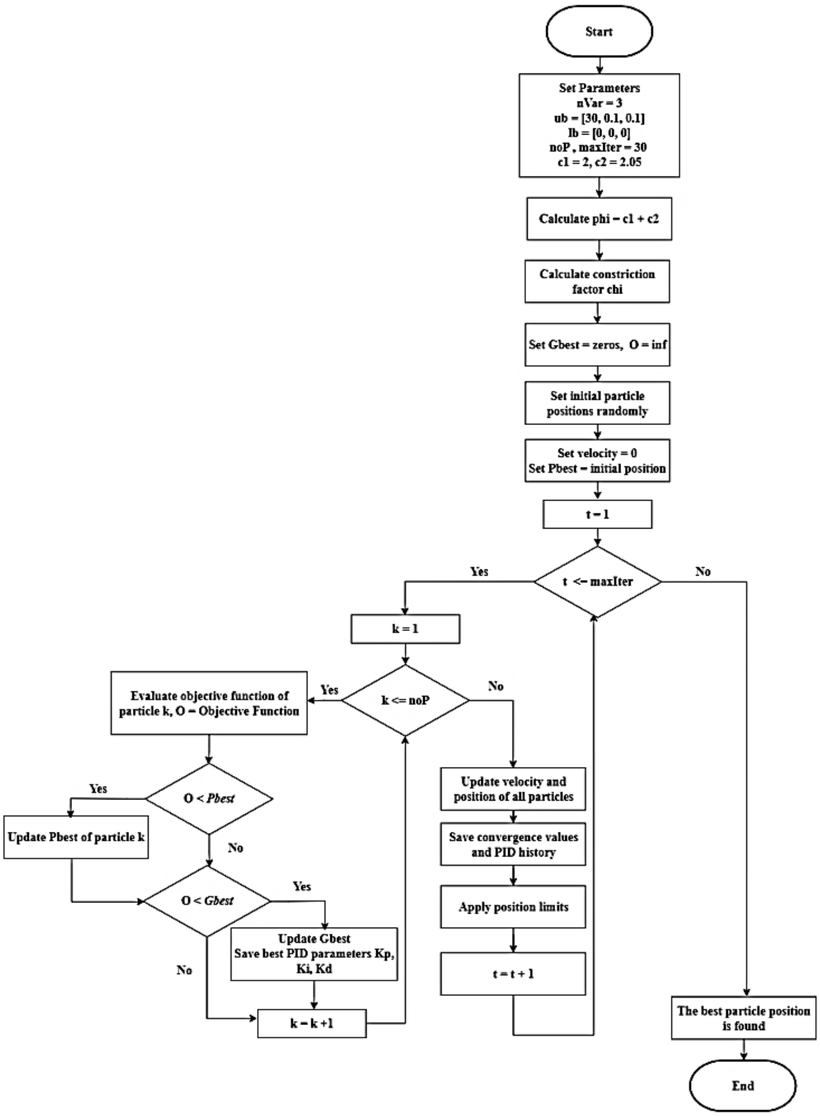

Fig. 8. Flowchart of PID controller design using the PSO method.

Table 1. Simulation results of PID parameter tuning for azimuth axis motor.

Number of Particles	Tuning Result			Rise Time (s)	Settling Time [s]	Overshoot [%]	ITSE
	P	I	D				
2	30	0.038	0.043	0.5685	0.7586	0	347.11
4	30	0.1	0	0.5691	0.7617	0.052	347.17
6	26.21	0.097	0.1	0.5697	0.7761	0	347.516
8	30	0.037	0.025	0.5685	0.7580	0	346.1

Table 2. Simulation results of PID parameter tuning for elevation axis motor.

Number of Particles	Tuning Result			Rise Time [s]	Settling Time [s]	Overshoot [%]	ITSE
	P	I	D				
2	15	0.1	0.013	0.3787	0.5298	0.0804	153.924
4	15	0.1	0.1	0.3795	0.5355	0.078	154.031
6	15	0.1	0.01	0.3786	0.5297	0.0785	153.920
8	15	0.1	0.01	0.3786	0.5297	0.0785	153.920

After performing variations in the number of particles and evaluating the ITSE objective function, tuning the PID parameters for the azimuth motor with eight particles yielded the best performance, with parameters of $K_p = 30$, $K_i = 0.0037$, and $K_d = 0.025$. For the elevation motor, the configuration with four particles gave the best results with parameters of $K_p = 15$, $K_i = 0.1$, and $K_d = 0.01$.

During the design phase, the PSO-based tuning is performed offline. By identifying the optimal gains through simulation before the deployment, the resulting coefficients are implemented as static values within the microcontroller. This approach ensures that the antenna tracker gets all the benefits from optimized control without requiring real-time computational resources for the PSO algorithm during flight operations.

2.5. Telemetry and Communication System

The communication architecture is specifically developed to feauture long-range, high bandwidth data exchange between the UAV and the GCS. This system utilizes a high gain FY-05A directional panel antenna (14 dBi) that operates at the 5.8 GHz frequency band to ensure reliable signal reception at extended ranges.

A. Communication Protocol and Hardware

OpenHD, an open-source platform, controls the data transmission that enables concurrent HD video and telemetry streaming through the modified Wi-Fi modules. The Micro Air Vehicle Link (MAVLink) protocol is used because this system offers a stable and consistent communication structure that purposively optimized for unmanned systems.

B. Data Acquisition and Uplink/Downlink Process

UAV gets spatial measurements from onboard sensors to start the telemetry process. These measurements include GPS for positional coordinates and a barometer for sea level altitude. These measurements are also encapsulated into MAVLink packets and transmitted via a 5.8 GHz digital radio link.

The directional FY-05A antenna, on the GCS side, captures the incoming signal, and the tracking system continuously controls the antenna to maintain boresight alignment with the UAV. The GCS is used to process the demodulated digital data in order to show real time parameters (latitude, longitude, and altitude). This process is used as the inputs for tracking algorithms.

C. Signal Mitigation and Tracking Integration

The GCS performs real-time coordinate transformations to maintain precise antenna pointing accuracy, and specifically to address the inherent path loss with the 5.8 GHz frequency band. The process begins by calculating the azimuth, where longitudinal and latitudinal differences are processed through Eqs. (1) and (2) to obtain directional components which are then integrated using Eq. (3). This process is conducted to determine the bearing relative to true north.

At the same time, the elevation angle is calculated using haversine formula in Eq. (6) to find the horizontal distance. Then, Eq. (7) applies trigonometric adjustment to know the altitude difference (f) between the UAV and the ground station. The resulting angular setpoints are transmitted to the microcontroller to control the stepper motors. This ensures precise synchronization between the antenna's orientation and the UAV's flight path. This continuous feedback loop maintains a stable, high-speed communication link. The summary of the data processing flow is shown in Fig. 9.

Fig. 9. illustrates the complete flowchart of data processing and transmission from UAV to antenna tracker, from initial sensor data acquisition on the UAV to the final motor actuation at the GCS. Through this figure, the real-time data flow can be simply overviewed. It points out the coordinate transformations and mathematical models described in Eqs. (1) through (7) are operationalized within the tracking software to maintain a continuous communication link.

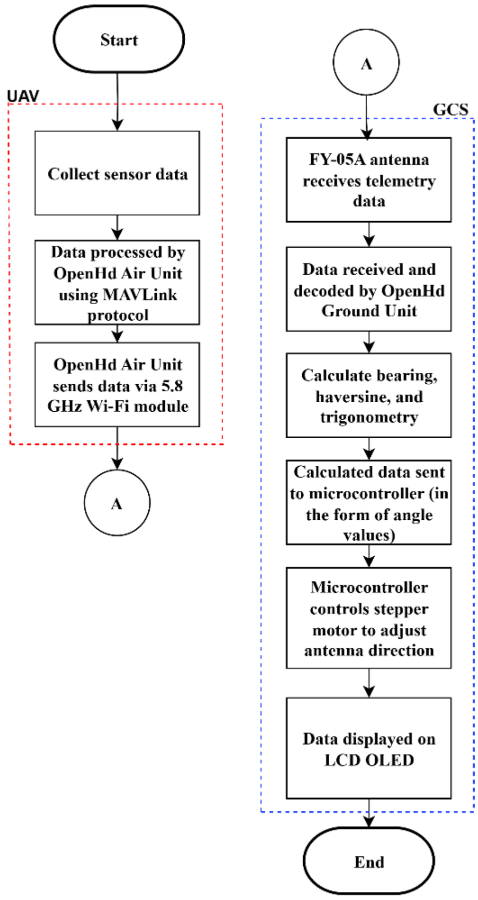

Fig. 9. Flowchart of data processing and transmission from UAV to antenna tracker.

3. RESULT AND DISCUSSION

3.1. Performance of Axis Motor Control

Manual evaluation is used in the system response of the elevation axis motor by applying step reference angles of 10°, 30°, and 90°. Table 3 shows the experimental results, showing key response parameters such as rise time, settling time, overshoot (OS), steady-state error (SSE), and the Integral of Time-weighted Squared Error (ITSE).

Table 3. Experimental results of system response for elevation axis motor

Ref [°]	Rise Time [ms]	Settling Time [ms]	OS [%]	SSE [°]	ITSE
10	966	2051	0.67	0.040	4.190
30	1863	2736	0.07	0.008	144.565
90	1980	3324	0.23	0.203	2508.482

To evaluate the relative performance of the proposed system, the test results at a 90° reference angle were compared to the previous studies. Based on the comparison, the study in

[34] demonstrated a settling time of 6231 ms and an overshoot of 2.6% for the elevation axis. Using identical test conditions, the system in this study reached a settling time of 3324 ms and an overshoot of only 0.23%. Overall, there is a 46.7% reduction in settling time and a decrease in overshoot by over 11.

This comparison shows a significant improvement in system stability and responsiveness. Additionally, the controller on the elevation axis demonstrates high accuracy with a maximum steady-state error (SSE) of only 0.203° at the 90° reference angle. This value is significantly smaller than the antenna's directional tolerance of ±20° beamwidth, confirming that the system is reliable to maintain antenna alignment with the UAV.

Theoretically, it is assumed that the UAV is located at a distance of d = 50 m from the antenna tracker. Based on Eq. (12), at this distance, the UAV can move vertically up to ±18.2 m from the antenna boresight and still stay within the signal coverage. Considering the measured SSE of 0.203°, the system can theoretically maintain UAV tracking at distances more than 5 km. Thus, the UAV does not vertically move more than 18.2 m.

$$a = d * \tan(\theta) \quad (12)$$

In addition, from the response test to the 90° reference input, the system showed an elevation motor rotation capability of 36.6°/s. Based on Eq. (13), the system can track a UAV vertical movement at a speed of approximately 31.75 m/s at 50 m without surpassing the antenna beamwidth coverage.

$$\omega_{max} = \frac{v}{R} \quad (13)$$

3.2. Performance of Azimuth Motor Control

The system response on the azimuth motor was evaluated by applying manual reference input angles of 10°, 30°, 90°, 210°, and 360°. The Table 4 shows the test results and system responses parameters summary, including rise time, settling time, overshoot (OS), steady-state error (SSE), and ITSE.

Table 4. Experimental results of system response for azimuth axis motor.

Ref [°]	Rise Time [ms]	Settling Time [ms]	OS [%]	SSE [°]	ITSE
10	730	1294	0.42	0.021	3.073
30	761	1285	0.41	0.023	35.970
90	1107	1794	0.07	0.023	899.220
210	2104	2916	0.05	0.033	23406.663
360	3505	4588	0.03	0.056	208584.680

In order to ensure its effectiveness, the system's performance was compared to the previous studies. At a 90° reference angle, the study in [34] showed a settling time of 1583 ms, but with a very high overshoot of 28.8%. While the proposed system's settling time at the same angle was longer in 1794 ms, it gave superior stability with a minimal overshoot of only 0.07%. In antenna tracking applications, minimizing overshoot is important to prevent target signal loss, making the proposed system significantly more reliable. Additionally, the system gives high accuracy with a maximum SSE of only 0.056°. This value is significantly smaller than the antenna pointing tolerance of ±40° beamwidth. It ensures the system to precisely maintain the antenna alignment with the UAV. Theoretically, it is assumed that the UAV is located at a distance of d = 50 m from the antenna tracker. Based on Eq. (12), at this distance, the UAV can move horizontally up to ±41.1 m from the antenna boresight and stay within the beamwidth coverage. With an SSE of 0.056°, the system can theoretically maintain UAV tracking at distances of more than 42 km. Therefore, the UAV remains on a straight trajectory without deviating more than 41.1 m.

3.3. Autonomous Monitoring Mission and Dynamic Accuracy

During the autonomous monitoring mission, the UAV followed a predefined flight path covering approximately 1 km at specified altitudes. The designed mission trajectory and the actual flight path showing speed variations from 1 m/s to 3 m/s are illustrated in Fig. 10.

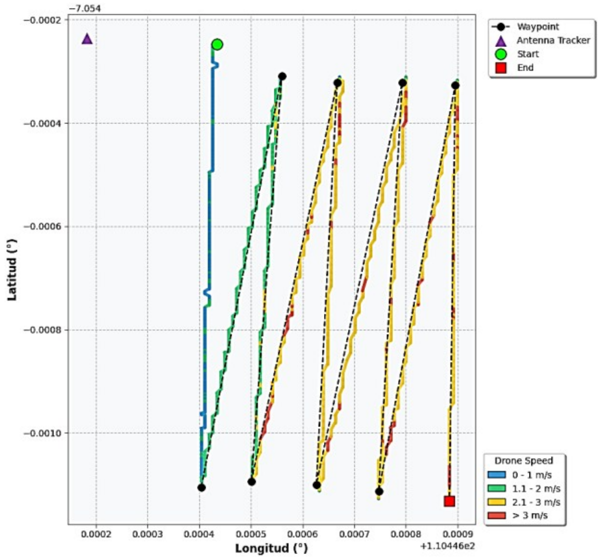

Fig. 10. Visualization of the actual UAV trajectory during the autonomous monitoring mission.

A. Dynamic Tracking Performance and Benchmarking

In order to ensure the scientific contribution and practicality of this study, the proposed PSO-PID antenna tracker was compared to several existing implementations. Table 5 shows the differences between this study and previous studies in terms of frequency bands, control strategies, and validation methods. Fig. 11 shows the system's dynamic response during the mission. Based on calculations using Eq. (14), the Mean Absolute Error (MAE) was recorded at 0.37° for the azimuth axis and 0.03° for the elevation axis.

$$MAE = \frac{1}{n} \sum_{i=1}^{n} |y_i - \hat{y}_i| \quad (14)$$

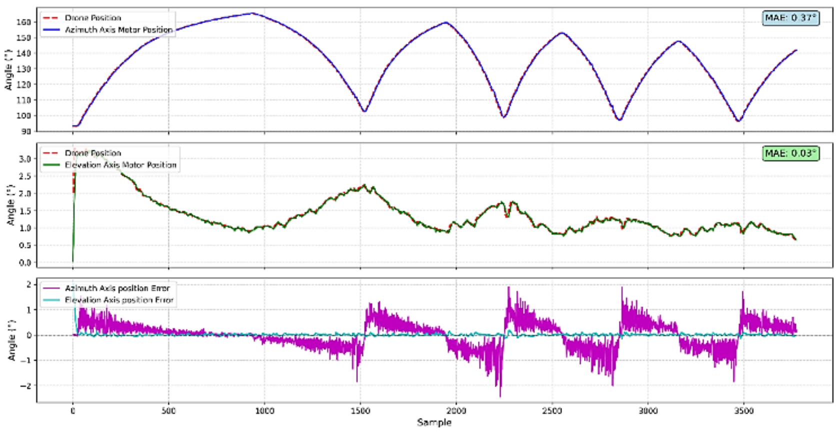

Fig. 11. System response of the antenna tracker.

Compared to [21], the proposed system is about 15 times more accurate in azimuth and 50 times in elevation. The azimuth error is higher because the UAV makes more horizontal moves when changing waypoints, yet its altitude changes are smoother. This causes fewer changes in elevation.

Table 5. Comparative summary of the proposed antenna tracker versus prior studies.

System / Reference	Freq. Band	Antenna Type	Controller	Tracking Error	Validation Scale
Proposed (This Work)	**5.8 GHz**	**Directional Panel FY-05A (14 dBi)**	**PSO-PID (ITSE)**	**MAE ≤0.48° (az), 0.03° (el); SSE 0.056° (az), 0.203° (el)**	**Real outdoor autonomous flight; 1 km range; UAV speed 0.1–3.0 m/s**
[21] Nugroho & Dectaviansyah (2018)	915–928 MHz	3-element Yagi (6 dBi)	PID (manual tuning)	Avg. error: 5.62° (az), 1.51° (el)	Real outdoor; UAV field test (quadcopter)
[29] Işcan et al. (2022)	Not specified	Not specified	Discrete Lyapunov-based proportional	±0.3° (pan), ±0.6° (tilt)	Simulation (MATLAB/Simulink) + STM32 lab; no UAV field test
[34] Jayadi et al. (2023)	Not specified	Not specified	PID (trial-and-error)	Settling: 6231 ms, Overshoot: 2.6% (el @ 90°)	Lab/indoor static test; no UAV field validation

B. Analysis of Maneuverability and UAV Speed

Based on Fig. 12, which shows the azimuth error plot, the error is highest when the UAV makes turns, shown by repeated spikes in the graph. This occurs because abrupt changes in UAV direction result in sudden variations in the azimuth reference for the antenna tracker. The system can effectively track the UAV's movement, as shown by the relatively small MAE value. Analysis was further conducted through the observation of the antenna tracker performance at different UAV speed ranges: 0.1–1 m/s, 1.1–2 m/s, and 2.1–3 m/s. Fig. 12 shows that the antenna tracker has an excellent tracking performance within the 0.1–1.0 m/s range with a mean absolute error (MAE) of 0.19°. Fig. 13 presents the performance at 1.1–2 m/s. It means that the system gives good tracking accuracy with an MAE of 0.33°. Meanwhile, Fig. 14 shows the performance at 2.1–3 m/s, where the system continues to track the UAV accurately, giving an MAE of 0.48°.

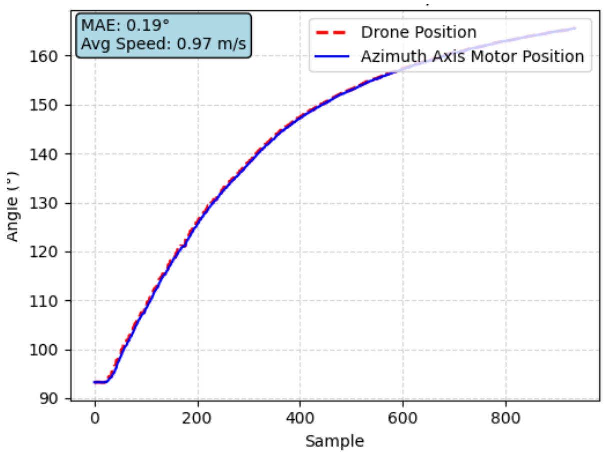

Fig. 12. Azimuth axis response at UAV speed of 0.1 m/s – 1 m/s.

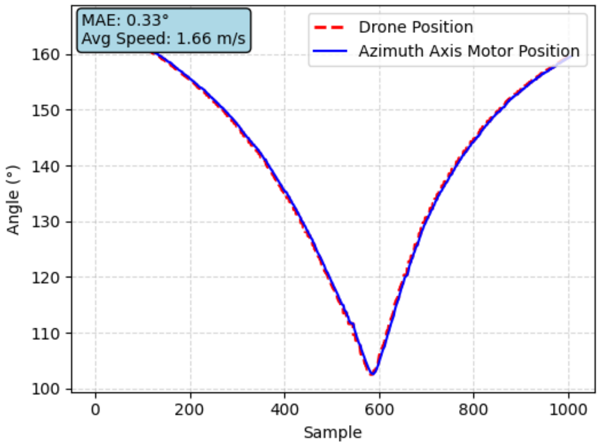

Fig. 13. Azimuth axis response at UAV speed of 1.1 m/s – 2.0 m/s.

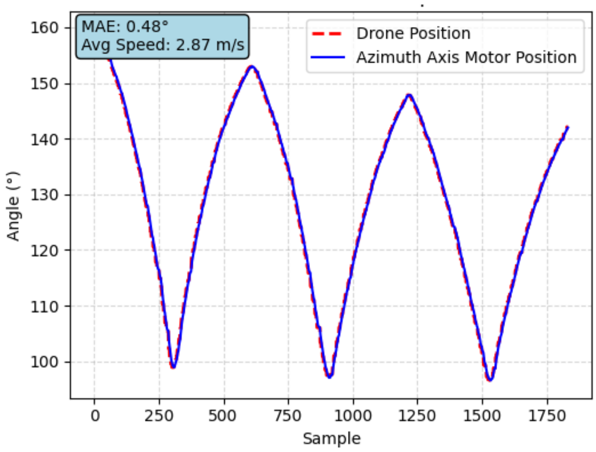

Fig. 14. Azimuth axis response at UAV speed of 2.1 m/s – 3.0 m/s.

Overall, the system is capable of accurately tracking UAVs in various speeds. When the UAV moves faster, the tracking error also increases, which can be seen from the higher MAE values. Based on calculations, an increase of 1 m/s in UAV speed leads to an approximate 0.164° increase in tracking error.

3.4. Telemetry Signal Quality and Field Validation

The signal quality of the communication system was evaluated through two phase: a static distance test and a dynamic autonomous monitoring mission. These tests aimed to compare the high-gain FY-05A directional panel antenna and a standard Holybro 433 MHz omnidirectional antenna. Traditional telemetry systems such as Holybro 433 MHz offer superior signal transmission for long data distances, but do not support the high bandwidth of HD video. This study utilized the 5.8 GHz band to cover these data requirements, despite its higher Free-Space Path Loss (FSPL). As a practical solution, an antenna tracker was implemented to maintain precise boresight alignment. Thus, it allows the high gain of a directional antenna to match 5.8 GHz signal attenuation and maintain connection stability that standard omnidirectional antennas cannot achieve.

To ensure a fair comparison during evaluation, both the 5.8 GHz and 433 MHz systems were set to the same transmission power of 20 dBm using OFDM modulation via the OpenHD platform. Additionally, both antennas were vertically polarized to reduce signal mismatch during UAV maneuvers, ensuring that the tracking performance was the main factor affecting link stability.

A. Comparative Static Distance Test

The performance of both antennas was measured with distances ranging from 100 m to 1000 m. Received Signal Strength Indicator (RSSI) at the GCS and the Remote RSSI (REMRSSI) at the UAV was the main indicator for this assessment. The results are summarized in Table 6.

Table 6. Experimental comparison of directional antenna (FY-05A) and omni-directional antenna (Holybro) at various distance.

Distance [m]	Directional (FY-05A)		Omni-directional (Holybro)	
	RSSI [dBm]	REMRSSI [dBm]	RSSI [dBm]	REMRSSI [dBm]
100	-63	-66	-64	-60
200	-68	-75	Disconnected	Disconnected
300	-70	-73	Disconnected	Disconnected
400	-73	-71	Disconnected	Disconnected
500	-75	-81	Disconnected	Disconnected
600	-77	-82	Disconnected	Disconnected
700	-76	-78	Disconnected	Disconnected
800	-75	-84	Disconnected	Disconnected
900	-75	-84	Disconnected	Disconnected
1000	-77	-83	Disconnected	Disconnected

The directional antenna gave a consistent and reliable link even at 1000 m. In contrast, the omnidirectional antenna lost connection beyond 100 m. This shows that the 14 dBi gain of the FY-05A successfully covers the significant path loss in the 5.8 GHz frequency band, which is otherwise limited in range when using conventional antennas.

B. Signaling Performance during Autonomous Mission

The stability of the link was further tested during the 1-km forest monitoring simulation. For the 5.8 GHz system, which handles both telemetry and high bandwidth HD video, high gain is essential for video clarity. The RSSI fluctuations for the directional antenna during the mission are shown in Fig. 15.

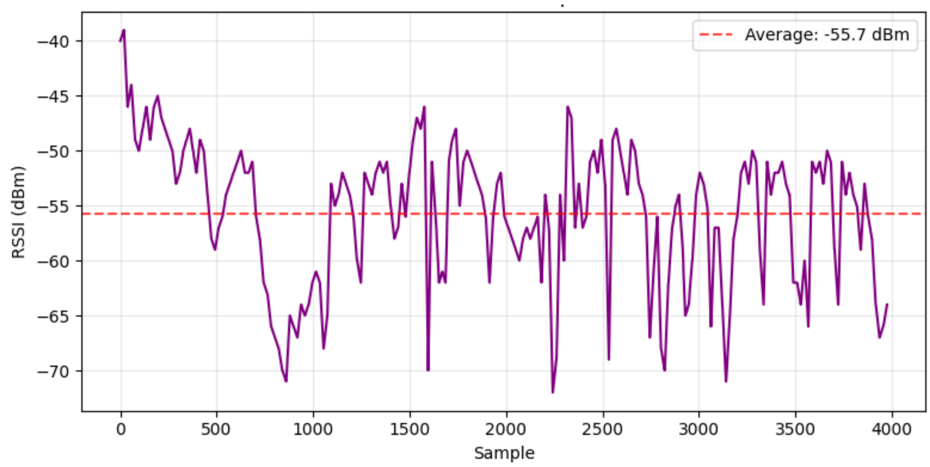

Fig. 15. RSSI graph during autonomous monitoring mission with directional antenna.

The RSSI for the directional antenna ranged from -38 to -71 dBm, with an average of -55.7 dBm. The intermittent declines in signal strength coincided with UAV turning maneuvers, which caused temporary misalignment between the UAV's transmission direction and the tracker's reception boresight. However, the antenna tracker's ability to rapidly reorient ensured that the signal recovered immediately once the maneuver was completed, maintaining a stable HD video feed.

Conversely, the 433 MHz omnidirectional antenna which only transmitted telemetry data exhibited much higher instability, as shown in Fig. 16. The RSSI fluctuated between 60 and -86 dBm, with an average of -72.3 dBm. As the UAV moved to the mission's perimeter, the signal weakened significantly due to distance and environmental obstacles. The average RSSI difference of 16.6 dBm proves that the tracking antenna system is much more reliable for long-range UAV operations with high bandwidth requirements.

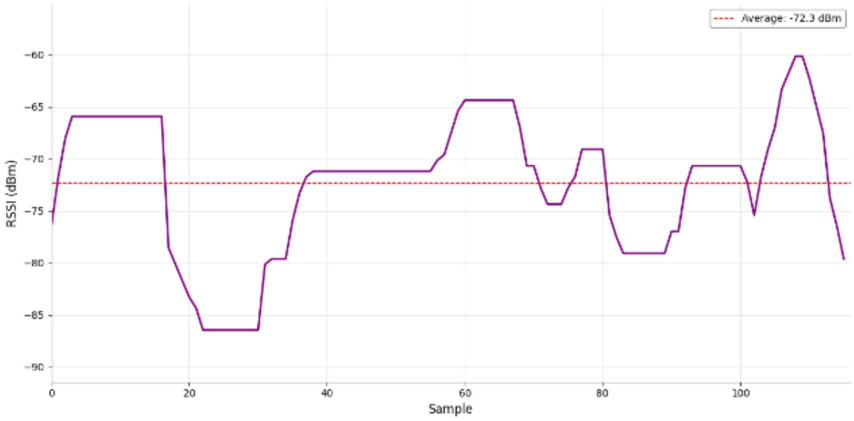

Fig. 16. RSSI graph during autonomous monitoring mission with omni-directional antenna.

4. CONCLUSIONS

This study has successfully developed and validated a high-precision UAV antenna tracker system which is optimized through Particle Swarm Optimization (PSO) with an Integral of Time-weighted Squared Error (ITSE) objective function. The experimental results show that the PSO-tuned PID controller significantly enhances dynamic stability and pointing accuracy. The system got a maximum steady-state error (SSE) of 0.203° for the elevation axis and 0.056° for the azimuth axis. During a 1-km autonomous flight mission, the tracker demonstrated exceptional performance with a Mean Absolute Error (MAE) of 0.37° (azimuth) and 0.03° (elevation).

The 5.8 GHz telemetry system, integrated with a 14-dBi directional panel antenna, effectively reduced high-frequency path loss. However, this stability was strictly dependent on the automated tracker. Because of the narrow beamwidth of high-gain antennas, any movement without real-time synchronization would cause immediate signal loss. By maintaining continuous boresight alignment, the proposed tracker achieved a stable average RSSI of -55.7 dBm. This enables high-bandwidth HD video transmission up to 1 km and significantly outperforms the standard 433 MHz omnidirectional system, which suffered connection losses beyond 200 m with a much lower average RSSI of -72.3 dBm.

Although the proposed system shows high reliability, there are still limitations to be taken into account in future research:

1. The current tests were conducted in open areas. Thus, future studies should test the tracker in more restricted areas like urban or dense forest areas where signal interference and multipath fading are high.

2. The system had good accuracy at UAV speeds up to 3 m/s. However, more testing is needed for faster fixed-wing UAVs for example during extreme flight maneuvers.
3. The current tracking system depends heavily on GPS data. Therefore, future improvements could integrate computer vision or an inertial navigation system (INS) to keep tracking stable if the GPS signal is lost or interrupted.
4. This study tested the system up to a limited distance of 1 km with limited UAV's battery. Although the system could work over longer distances, future work should follow local transmission power rules and solve possible signal quality loss (SNR) at farther ranges.

Acknowledgement: The authors would like to thank the Department of Electrical Engineering, Faculty of Engineering, Universitas Diponegoro, for the facilities and support provided in conducting this research.

REFERENCES

[1] S. Bhattacharya, A. Singh, "Revolutionizing healthcare: navigating the trajectory of unmanned aerial vehicles from history to horizon," May 01, 2024, *Elsevier B.V.* doi: 10.1016/j.mjafi.2023.11.003.

[2] S. Mohsan, N. Othman, Y. Li, M. Alsharif, M. Khan, "Unmanned aerial vehicles (UAVs): practical aspects, applications, open challenges, security issues, and future trends," 2023, *Springer Science and Business Media Deutschland GmbH*. doi: 10.1007/s11370-022-00452-4.

[3] A. Yazıcı, G. Ömür, D. Celik, "Applications and future perspectives of swarm intelligence in unmanned and autonomous systems," *Sosyal Mucit Academic Review*, 2024, doi: 10.54733/smar.1555925.

[4] A. N. Barve *et al.*, "Advancing precision agriculture: the role of UAVs and drones in sustainable farming," *Asian Research Journal of Agriculture*, vol. 17, no. 4, pp. 987–992, 2024, doi: 10.9734/arja/2024/v17i4611.

[5] S. Pathak, S. Acharya, S. Bk, G. Karn, U. Thapa, "UAV-based topographical mapping and accuracy assessment of orthophoto using GCP," *Mersin Photogrammetry Journal*, vol. 6, no. 1, 2024, doi: 10.53093/mephoj.1350426.

[6] M. Ghamari, P. Rangel, M. Mehrubeoglu, G. Tewolde, R. Sherratt, "Unmanned aerial vehicle communications for civil applications: a review," *Institute of Electrical and Electronics Engineers Inc.*, 2022, doi: 10.1109/ACCESS.2022.3208571.

[7] L. Lin, R. Shangguan, H. Ge, Y. Liu, Y. Zhou, Y. Zhou, "Mutual identity authentication based on dynamic identity and hybrid encryption for UAV–GCS communications," *Drones*, vol. 9, no. 6, 2025, doi: 10.3390/drones9060422.

[8] Y. Lau, M. Ang, "A novel link failure detection and switching algorithm for dissimilar redundant UAV communication," *Drones*, vol. 5, no. 2, 2021, doi: 10.3390/drones5020048.

[9] Y. Ko, J. Kim, D. Duguma, P. Astillo, I. You, G. Pau, "Drone secure communication protocol for future sensitive applications in military zone," *Sensors*, vol. 21, no. 6, pp. 1–25, 2021, doi: 10.3390/s21062057.

[10] M. Sadiq, C. Ruan, H. Nawaz, S. Ullah, W. He, "Horizontal polarized dc grounded omnidirectional antenna for uav ground control station," *Sensors*, vol. 21, no. 8, Apr. 2021, doi: 10.3390/s21082763.

[11] A. Koru, J. Chang, Y. Wan, "RSSI-based distributed control to align directional antenna pairs for UAV communication," *IEEE/ASME Transactions on Mechatronics*, vol. 29, no. 4, pp. 2877–2885, 2024, doi: 10.1109/TMECH.2024.3403911.

[12] T. Yu, K. Kajiwara, K. Araki, K. Sakaguchi, "Spectrum sharing between directional-antenna-equipped UAV system and terrestrial systems," IEEE 12th Annual Computing and Communication Workshop and Conference, 2022, doi: 10.1109/CCWC54503.2022.9720775.

[13] M. Sharma, I. Farhat, C. Liu, N. Sehad, W. Hamidouche, M. Debbah, "Real-time immersive aerial video streaming: a comprehensive survey, benchmarking, and open challenges," *IEEE Open Journal of the Communications Society*, vol. 5, pp. 5680–5705, 2024, doi: 10.1109/OJCOMS.2024.3455763.

[14] T. Hsu, R. Ju, G. Horng, "enhanced adaptive video streaming for resource-constrained uavs through dynamic region-of-interest tile swapping," International Conference on Applied System Innovation, 2024, doi: 10.1109/ICASI60819.2024.10547839.

[15] Z. Liu, M. Wang, F. Chen, Q. Lu, "Edge-assisted intelligent video compression for live aerial streaming," *IEEE Transactions on Green Communications and Networking*, vol. 6, no. 3, pp. 1613–1623, 2022, doi: 10.1109/TGCN.2022.3172900.

[16] P. Chandhar, E. Larsson, "Massive MIMO for connectivity with drones: case studies and future directions," *IEEE Access*, vol. 7, pp. 94676–94691, 2019, doi: 10.1109/ACCESS.2019.2928764.

[17] R. Anzum *et al.*, "A Multiwall path-loss prediction model using 433 MHz LoRa-WAN frequency to characterize foliage's influence in a malaysian palm oil plantation environment," *Sensors*, vol. 22, no. 14, 2022, doi: 10.3390/s22145397.

[18] M. Hariyadi, J. Fadila, "Evaluation of unmanned aerial vehicle (UAV) control range system using lora-based communication system using path loss," *Fountain of Informatics Journal*, vol. 7, no. 2, pp. 57–63, 2022, doi: 10.21111/fij.v7i2.7571.

[19] Z. Akhter, R. Bilal, K. Telegenov, E. Feron, A. Shamim, "Indigenously developed HD video transmission system for UAVs employing a 3 × 3 MIMO antenna system," *IEEE Open Journal of Antennas and Propagation*, vol. 3, pp. 940–947, 2022, doi: 10.1109/OJAP.2022.3198289.

[20] A. Mahmood, K. Al-Bayati, R. Szabolcsi, "Optimizing antenna azimuth position control using fuzzy PD, fuzzy PD-I, and fuzzy PD-plus-I controllers," *Nanotechnol Percept*, vol. 20, no. 3, pp. 18–32, 2024, doi: 10.62441/nano-ntp.v20i3.2.

[21] G. Nugroho, D. Dectaviansyah, "Design, manufacture and performance analysis of an automatic antenna tracker for an unmanned aerial vehicle (UAV)," *Journal of Mechatronics, Electrical Power, and Vehicular Technology*, vol. 9, no. 1, pp. 32–40, 2018, doi: 10.14203/j.mev.2018.v9.32-40.

[22] L. Alwal, P. Kihato, S. Kamau, "Design of neuro-fuzzy system controller for DC servomotor based satellite tracking system," *IOSR Journal of Electrical and Electronics Engineering*, vol. 11, no. 04, pp. 89–102, 2016, doi: 10.9790/1676-11040389102.

[23] M. Massoud, P. Alves, J. Libby, "Enhancing dual-loop pressure control in pneumatic soft robotics with a comparison of evolutionary algorithms for PID & FOPID controller tuning," *IEEE Robot Autom Lett*, vol. 10, no. 6, pp. 6119–6126, 2025, doi: 10.1109/LRA.2025.3563163.

[24] Y. Wu, H. Xiao, H. Xu, H. Chen, Y. Zhang, Q. Yuan, "Robust MEMS temperature control platform with GA PSO - Fuzzy PID control," *IEEE Sensors Journal*, 2025, doi: 10.1109/JSEN.2025.3585178.

[25] H. Sarir, "Application of fuzzy logic controller and PID optimization control strategy based on particle swarm optimization (PSO) for inventory management," International Symposium on Advanced Electrical and Communication Technologies, 2020, doi: 10.1109/ISAECT50560.2020.9523666.

[26] A. Suryamanggala, D. Wicaksono, E. Rahayu, "Design and comparative study among antennas of gcs for telemetry communication system of UAV," *International Journal of Information Technology and Electrical Engineering*, vol. 3, no. 4, pp. 9, 2019, doi: 10.22146/ijitee.50866.

[27] J. Stevenson, S. O'Young, L. Rolland, "Beyond line of sight control of small unmanned aerial vehicles using a synthetic environment to augment first person video," Procedia Manufacturing, 2015, doi: 10.1016/j.promfg.2015.07.146.

[28] M. Hameed, Z. Khalaf, "a comprehensive review for aircraft detection techniques utilizing deep learning," *Iraqi Journal for Electrical and Electronic Engineering*, vol. 21, no. 2, pp. 216–236, 2025, doi: 10.37917/ijeee.21.2.21.

[29] M. İşcan, A. Taş, B. Vural, A. Ozden, C. Yılmaz, "Antenna tracker design with a discrete lyapunov stability based controller for mini unmanned aerial vehicles," *International Journal of*

Multidisciplinary Studies and Innovative Technologies, vol. 6, no. 1, p. 77, 2022, doi: 10.36287/ijmsit.6.1.77.

[30] K. Patel, Y. Sojitra, "Autonomous surveillance drone," *International Journal of Scientific Research in Science, Engineering and Technology*, vol. 12, no. 2, pp. 750–754, 2025, doi: 10.32628/ijsrset25122202.

[31] H. Goud *et al.*, "PSO based multi-objective approach for controlling PID controller," *Computers, Materials and Continua*, vol. 71, no. 2, pp. 4409–4423, 2022, doi: 10.32604/cmc.2022.019217.

[32] S. Gupta *et al.*, "Metaheuristic optimization techniques used in controlling of an active magnetic bearing system for high-speed machining application," *IEEE Access*, vol. 11, pp. 12100–12118, 2023, doi: 10.1109/ACCESS.2023.3241854.

[33] R. Mendes, J. Kennedy, J. Neves, "The fully informed particle swarm: Simpler, maybe better," *IEEE Transactions on Evolutionary Computation*, vol. 8, no. 3, pp. 204–210, 2004, doi: 10.1109/TEVC.2004.826074.

[34] A. Jayadi, F. Adhinata, J. Sembiring, C. Adhi, W. Selsily, A. Amiruddin, "Design and implementation of a PID control system on a UAV tracker antenna," International Conference on Advanced Mechatronics, Intelligent Manufacture and Industrial Automation, 2023, doi: 10.1109/ICAMIMIA60881.2023.10427743.